Complex ligand adsorption on 3D atomic surfaces of synthesized nanoparticles investigated by machine-learning accelerated ab initio calculation

Dohun Kang[1,2,#], Sungin Kim[1,3,#], Junyoung Heo[1,3], Dongjun Kim[1], Hyeonhu Bae[4], Sungsu Kang[1,3], Sangdeok Shim[5,], Hoonkyung Lee[4,*], Jungwon Park[1,3,6,7,*]*

[1] School of Chemical and Biological Engineering, and Institute of Chemical Processes, Seoul National University, Seoul 08826, Republic of Korea

[2] Department of Materials Science and Engineering, Northwestern University, Evanston, Illinois 60208, USA

[3] Center for Nanoparticle Research, Institute for Basic Science (IBS), Seoul 08826, Republic of Korea

[4] Department of Physics, Konkuk University, Seoul 05029, Republic of Korea

[5] Department of Chemistry, Sunchon National University, Suncheon 57922, Republic of Korea

[6] Institute of Engineering Research, College of Engineering, Seoul National University, 1 Gwanak-ro, Gwanak-gu, Seoul 151-742, Republic of Korea

[7] Advanced Institutes of Convergence Technology, Seoul National University, 145, Gwanggyo-ro, Yeongtong-gu, Suwon-si, Gyeonggi-do, 16229, Republic of Korea

KEYWORDS: Nanoparticle-ligand interaction, Machine-learning-accelerated DFT, 3D atomic structure, Large ligand system, van der Waals interaction

ABSTRACT: Nanoparticle surfaces are passivated by surface-bound ligands, and their adsorption on synthesized nanoparticles is complicated because of intricate and low-symmetry surface structures. Thus, it is challenging to precisely investigate ligand adsorption on synthesized nanoparticles. Here, we applied a machine-learning-accelerated ab-initio calculation into experimentally resolved 3D atomic structures of Pt nanoparticles to analyze the complex adsorption behavior of polyvinylpyrrolidone (PVP) ligands on synthesized nanoparticles. Different angular configurations of the large-sized ligands are thoroughly investigated to understand adsorption behaviors onto the various surface-exposed atoms with intrinsic low-symmetry. It is revealed that long-range van der Waals interaction (E_{vdW}) shows weak negative relationship against generalized coordination number ($\overline{CN}$), in contrast to the positive relationship in short-range direct bonding (E_{bind}), which attenuates the correlation between ligand binding energy (E_{ads}) and $\overline{CN}$. In addition, the PVP ligands favor to adsorb at which the long-range vdW interaction with surrounding surface structure is maximized. Our results highlight the significant contribution of vdW interactions and importance of local geometry of surface atoms to adsorption behavior of large-sized ligands on synthesized nanoparticle surfaces.

(TOC graphic)

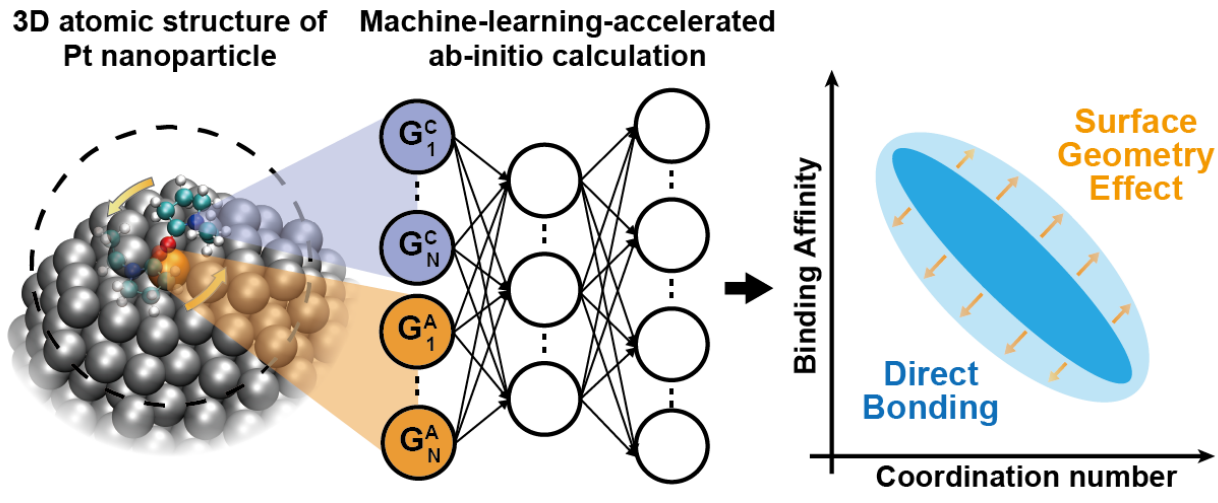

TEXT:

Surface-bound ligands determine structures of colloidal nanoparticles by regulating surface energy and growth pathway in the synthesis. In addition, physicochemical properties of synthesized nanoparticles are sensitive to the binding type and surface distribution of ligands[1-3]. There are different types of ligands used in the synthesis of nanoparticles, including polymers, organic molecules, inorganic complexes, and metal ions. Among them, polymers such as polyvinylpyrrolidone (PVP) are widely used to direct structures of metal nanoparticles, exploiting their preferential adsorption on different crystallographic surfaces[4-6].

Several experimental methods including infrared spectroscopy, nuclear magnetic resonance spectroscopy, and x-ray photoelectron spectroscopy are extensively used to investigate the ligand-binding chemistry on the nanoparticle surface[7-10]. However, they are based on spectroscopic information from nanoparticle ensemble and have limitation in investigating ligand interactions in a single particle level. Theoretical calculations based on quantum mechanics are employed to understand the adsorption chemistry of ligands with high accuracy[10-14], but are not yet readily applicable to the synthesized nanoparticles with complex surface structures and large-sized ligand system. Complex surfaces of synthesized nanoparticles having low-symmetry surface atoms, edges, and corners require extremely large computation resources. In addition, large-sized ligand systems have configurational degree of freedom along the different adsorbed direction and complex binding modes including van der Waals interaction.

Recently, several sampling methods based on machine learning have been proposed for fast and precise computation of the adsorption energy on the surface of nanoparticles. They are successful with small molecular adsorbates such as H, CO and HCHO[15-17]. The accuracy and efficiency demonstrated by artificial neural network (ANN) prediction for small molecules encourage us to investigate complex surface interactions of polymer ligands used in the

synthesis of nanoparticle by ANN. Here, we studied ligand binding characteristics in a synthesized nanoparticle-ligand system, Pt nanoparticles passivated by PVP ligands, using a machine-learning-accelerated ab-initio calculation. We applied ANN to the realistic 3D atomic structure of synthesized nanoparticles that we directly analyzed from their colloidal phase with a precision of 19 pm. This enabled the efficient scanning of binding interactions of a large-sized ligand on intrinsically disordered surfaces of colloidal nanoparticles without extended computation for structure relaxation. As a result, the energy, modes, and orientations of ligand bindings were thoroughly investigated for 1334 surface atomic sites of 6 Pt nanoparticles with a high precision. The results reveal that the short-range direct bonding and long-range van der Waals interaction of PVP are differently affected by the local coordination number of the surface-exposed atom and surrounding geometry, contributing to overall binding affinity of PVP on surfaces of synthesized Pt nanoparticles. In addition, it is found that the contribution from van der Waals interaction is important in the passivation of the nanoparticle surfaces by long ligand such as PVP polymers.

Realistic 3D atomic structures of individual single-crystalline Pt nanoparticles were obtained by the Brownian one-particle reconstruction method[18,19], revealing that structures of the PVP-passivated Pt nanoparticles are nonuniformly deviated from the bulk face-centered-cubic structure of Pt (Figures 1a,b). Surface structures of the synthesized Pt nanoparticles are complicated due to the irregular shapes of islands, resulting in diverse distribution of generalized coordination number ($\overline{\mathrm{CN}}$) that indicates distinct local geometry of a surface atom (Figure 1a). It implies that ligands could strongly interact with surface atoms and that the way they passivate the surface is complicated. In addition, the various surface structures cover much broader training space for ANN compared to model nanoparticles, which improves the accuracy of prediction for ligand adsorption behavior on Pt nanoparticles (Figure S1). From 3D atomic structures, surface atoms were defined as ones that have coordination number (CN)

≤ 9 and meet surface vector criteria (Figure S2 and see Methods in Supporting Information).

The Pt cluster clipped with a cutoff of 10 Å well represents the adsorption behavior of PVP on the Pt surface as shown in the benchmark calculation (Figure S3). It was modeled that a PVP monomer consists of a pyrrolidone ring, and an ethane group could bind to the top of Pt binding sites. The density functional theory (DFT) was corrected with DFT-D3 method to analyze complex PVP adsorption behavior composed of short-range direct bonding energy (E_{bind}) and long-range van der Waals interaction energy (E_{vdW}) (Figure 1c). The degree of freedom from the azimuthal binding angle was considered. Training data for ANN was constructed by extensive DFT calculations for PVP adsorption. Configurations of 1,386 representing 231 surface atoms of Pt nanoparticle 1 in Figure 1 including azimuth-rotated PVP orientations with 60-degree intervals for each site were initially screened. Among them, 452 configurations where PVP could not access were removed from data. In addition, 32 configurations were also excluded, which showed direct bonding by nitrogen atom of PVP. This binding mode is often observed for larger nanoparticles (~8.4 nm) while it is negligible for smaller nanoparticles (~6.4 nm and smaller) where carbonyl binding mode is dominant[10]. Thus, oxygen-binding mode of 902 configurations was eventually utilized for the training process.

The symmetry function was used for the input feature to predict the adsorption energy of PVP on the Pt adsorption center as shown in Figure 1d[20]. To handle the degree of freedom of azimuthally θ-rotated PVP, a characteristic point that represents local geometry information from PVP orientation was assigned. The characteristic vector was defined as the projection of Pt adsorption center to the nitrogen atom (Pt-N vector in Figure 1d) on the surface of Pt cluster (see Methods). The characteristic point was defined as the point 2.0 Å away from the adsorption center in the direction of the characteristic vector. The distance between the adsorption center and the characteristic point was determined by a 5-fold cross-validation (Supplementary Table

1). We calculated 40 symmetry functions from the adsorption center and characteristic point (12 for the radial part and 28 for the angular part) and concatenated them to make an input feature with 80 dimensions. The produced input feature was used by a two-layered fully connected neural network with 4412 hidden parameters to predict the E_{vdW} and E_{bind} separately. By using ANN, the angular adsorption energy profile of PVP on the various Pt nanoparticle surface structures can be deduced as shown in Figure 1e. Since ligands can dynamically interact with the metal nanoparticle surface by adsorption and desorption processes[9], the θ-averaged adsorption energy is used to represent the binding affinity of PVP to Pt adsorption centers.

The dataset with a total of 902 configurations was split into 722 data for the training set, 90 data for the validation set, and 90 data for the test set with the same coordination group ratio as the original dataset. We kept track of validation data for adjusting the learning rate with the learning rate scheduler to prevent overfitting. The evolution of training and validation error during the training epoch is shown in Figure S4. Training was early stopped at epoch 716, with 0.2169 eV root mean square error (RMSE) for the training set and 0.2250 eV RMSE for the validation set. Figures 2a,b shows the prediction result for the test set with 0.0519 eV and 0.0708 eV RMSE for E_{vdW} and E_{bind}, an error level comparable to those of a previous work for the adsorption of simple adsorbates (CO and HOCO)[16].

The surface atoms of each synthesized Pt nanoparticle 1 to 6 are displayed with a color gradient according to θ-averaged E_{bind}, E_{vdW} and E_{ads} assigned for each surface atom, respectively (Figures 2c,d, and Figure S5). For the E_{bind} and E_{ads} maps, adsorption centers on terrace show low binding energy, while others on edges and kinks show high binding energy. This result is consistent with previous results obtained from an ideal Pt surface[10]. However, E_{vdW} maps show higher binding energies on edges and kink compared to atoms on terrace. In addition, the distributions of averaged E_{bind} for each nanoparticle are different to those of averaged E_{vdW} (Figures S6 and S7). As shown in histograms of the averaged E_{bind} and E_{vdW} for

each nanoparticle, the energy distributions of E_{bind} are close to bimodal shape, while those of E_{vdW} are close to unimodal distribution. We calculated bimodality index (BI) for the energy distributions, representing the level of bimodal distribution, which shows that the distributions of E_{bind} have higher BI than those of E_{vdW} for all Pt nanoparticles (Figure S8 and see Methods in Supporting Information). These findings indicate that the two types of ligand binding modes are differently affected by Pt surface structures.

CN and generalized CN ($\overline{CN}$) are descriptors associated with chemical activities of surface atoms. It is known that CN and $\overline{CN}$ show strong linear relationship with adsorption energies of simple adsorbates such as O, O_2, OOH, and OCH_3 on high-symmetry metal nanoparticles[21-25]. However, unlike the simple adsorbates, the correlation between ANN-predicted averaged PVP adsorption energy (E_{ads}) and $\overline{CN}$ of an adsorption center shows weak positive relationship of linear correlation with Pearson correlation coefficient (r) of ~0.656 (Figure 3a).

As following the different trends of energy distributions in Figures 2c and 2d, averaged E_{bind} and E_{vdW} show different correlation with $\overline{CN}$ (Figures 3b,c). The correlation between E_{bind} and $\overline{CN}$ is highly linear with positive trend because direct bonding of PVP by the O atom of carbonyl group is predominantly governed by the degree of dangling bonds of the adsorbed Pt surface atom[26]. On the other hand, E_{vdW} shows weak negative relationship against $\overline{CN}$. Since the long-range interactions with surrounding Pt surfaces are also involved in the pyrrolidone ring and ethane group, E_{vdW} does not have noticeable relationship to the $\overline{CN}$ which is relevant to the coordination environment of an adsorption center. These different correlations with $\overline{CN}$ indicate that the weak positive relationship between the binding energy and $\overline{CN}$ is attributed to the van der Waals interactions of the large-sized ligands and the long-range interaction significantly contributes to the adsorption between large-sized ligands and complex surfaces of nanoparticles. Note that the Pearson correlation coefficient of E_{bind} to $\overline{CN}$ is still lower than

the one from ideal structures studied in previous reports because of the low-symmetry structure of synthesized Pt nanoparticles[22].

The negative relationship of E_{vdW} to the $\overline{CN}$ indicates that the pyrrolidone ring and ethane group strongly interact with the surrounding Pt surfaces when PVP binds to the Pt adsorption center with high $\overline{CN}$, such as terrace and step, whereas weakly interact when adsorption centers have low $\overline{CN}$ values, such as edge and corner. Since the long-range interaction is predominantly governed by the degree of contact between the PVP ligand and Pt surface, energy profiles along the different angular configuration of the PVP show that the energy deviation of E_{vdW} is larger than that of E_{bind} (Figure S9). Thus, the configuration of adsorbed PVP on the Pt surfaces with the lowest value of E_{vdW}, meaning the most stable van der Waals interaction, is required to investigate the relationship of E_{vdW} to $\overline{CN}$. For the adsorption directions with the lowest E_{vdW}, the characteristic vectors (the projection of the Pt-N vector on Pt surface, Figure 1c) are visualized as yellow arrows on the 3D atomic maps of Pt nanoparticles (Figures 4a,c, and e).

The adsorption directions on the Pt nanoparticle surfaces with the lowest E_{vdW} have following tendency. First, when the PVP ligands are directly bind to the terrace atoms of islands, they are more likely to direct toward the near terrace atoms (Figures 4a,b, and Figure S10). Second, the PVP ligands binding on the edge and corner atoms favor to locate toward the steps nearby (Figures 4c,d, and Figure S11). Third, PVP ligands binding on the adsorption centers under the islands tend to adsorb toward the steps nearby (Figures 4e,f, and Figure S12). These results indicate that a way to maximize the degree of contact of PVP ligands depends on the type of adsorption centers, which leads to the weak negative relationship between E_{vdW} and $\overline{CN}$. In addition, comparing the adsorption direction of each PVP ligand with the lowest E_{bind} and E_{vdW} to the adsorption direction with the lowest E_{ads}, the configurational similarity with the lowest E_{vdW} is higher than that of the lowest E_{bind} (Figure S13). It indicates that the PVP ligands favor

to adsorb at which the long-range vdW interaction with surrounding surface structure is maximized. In other words, surrounding surface geometry of an adsorption center is important in determining the most stable configuration of binding PVP ligands on low-symmetry surface structure of Pt nanoparticles.

PVP adsorption behavior on several adsorption centers with the same CN and similar $\overline{\mathrm{CN}}$ was carefully examined to represent the influence of surrounding surface geometry to the adsorption energy. Two adsorption centers for each particle with the same CN are colored in blue and orange (Figures 5a,b). Although each pair shows similar $\overline{\mathrm{CN}}$ values, the averaged adsorption energy of each adsorption center differs more than 0.1 eV (Figure 5b). It is because the local surface geometry surrounding the adsorption center is different as shown in the top view and side view (Figures 5a,b). In detail, the local surface geometry around the higher binding energy site shows a flat surface, while the lower binding energy site is surrounded by kinks and edges. It implies that the flat pyrrolidone ring of PVP favors neighboring flat surfaces with high van der Waals interaction. The binding energy for the sites even with the same $\overline{\mathrm{CN}}$ also shows difference in its angular profile (Figure 5c). The large difference of adsorption energies at the specific configurational angle is also shown in the results of the DFT calculation (Table S2). The results demonstrate that the adsorption energy of PVP ligands is significantly affected by each surrounding geometry.

In summary, we calculated the adsorption energy of PVP ligand on synthesized Pt nanoparticles and analyzed its adsorption behavior through machine-learning-accelerated ab-initio calculation. Using experimentally resolved atomic structures of nanoparticles provides sufficiently diverse sampling data for learning adsorption tendency on realistic nanoparticle surfaces and enables accurate prediction for surface chemistry. Our results reveal that the van der Waals interactions of the PVP with Pt surfaces induce weak positive relationship between adsorption energy and $\overline{\mathrm{CN}}$, which indicates the significance of surrounding surface structures

of adsorption centers when adsorbed with large-sized ligands. The introduced method utilizing machine-learning-accelerated ab-initio calculation and experimentally analyzed surface atomic structures suggests a new low-cost and high-precision computational approach for studying surface chemistry and catalytic activity of nanoparticles.

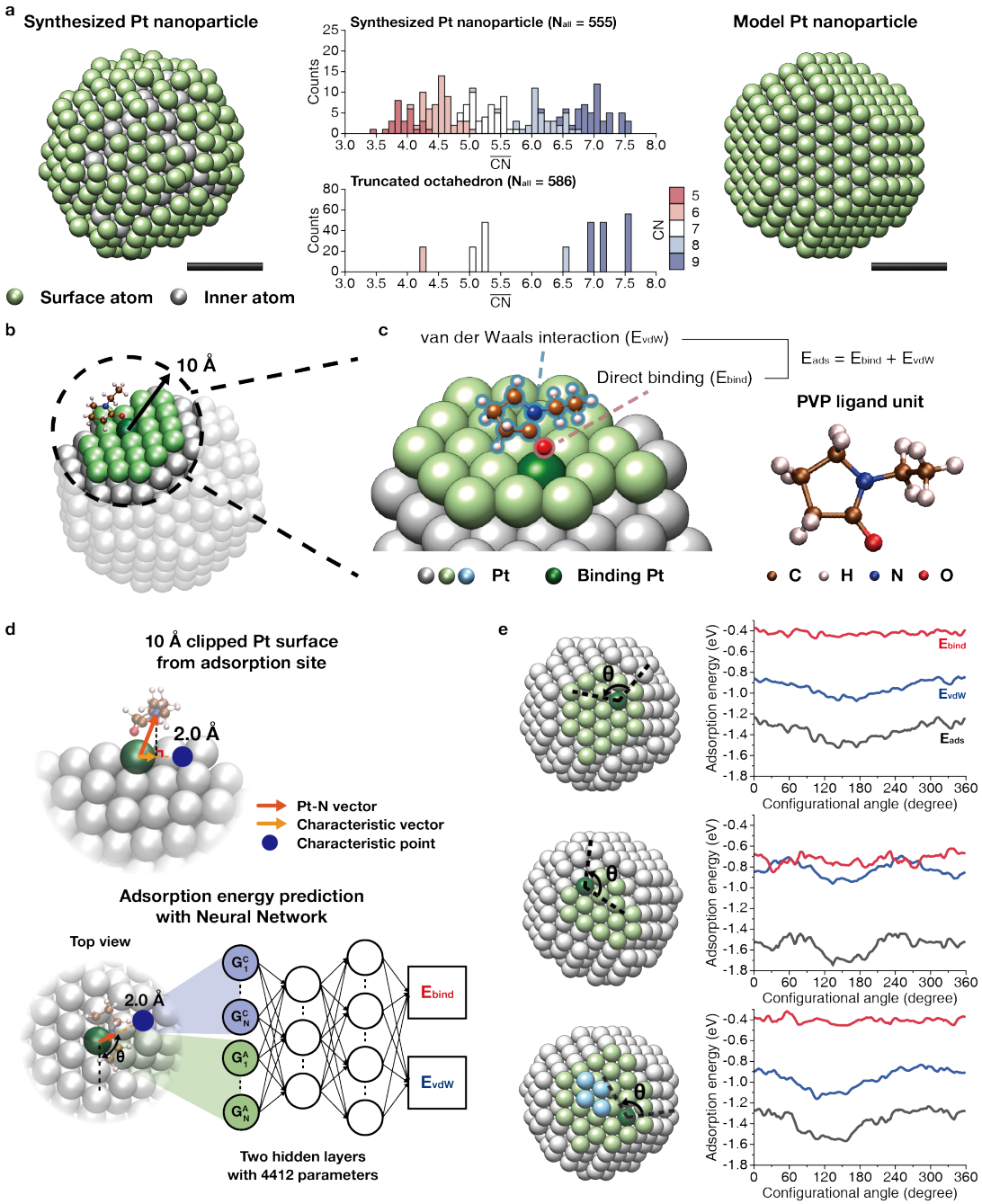

Figure 1. Scheme for machine-learning-accelerated ab-initio calculation. (a) Representative 3D structure of synthesized and model nanoparticles shown in left and right side, respectively. Histograms for the $\overline{CN}$ of surfaces atoms on the both nanoparticles are presented in the middle panel. The histograms of synthesized and model nanoparticles are shown in top and bottom, respectively. (b) The surface structure of PVP ligand protected Pt nanoparticle is clipped around 10 Å. (c) DFT-D3 calculated ligand binding energy (E_{ads}) is used for training set. (d)

Local geometric information is extracted as a set of symmetry functions from the adsorption site (green atom, G_i^N) and characteristic point (blue point, G_i^C) where the orientation of PVP monomer, θ, is reflected. Each of the two hidden layers of the fully connected neural network consists of 30 nodes and 60 nodes, respectively. (e) The angular adsorption energy profiles of PVP ligand on the different types of surface structures of particle 1 can be predicted by ANN. Red, blue and black lines indicate E_{bind}, E_{vdW} and E_{ads}, respectively.

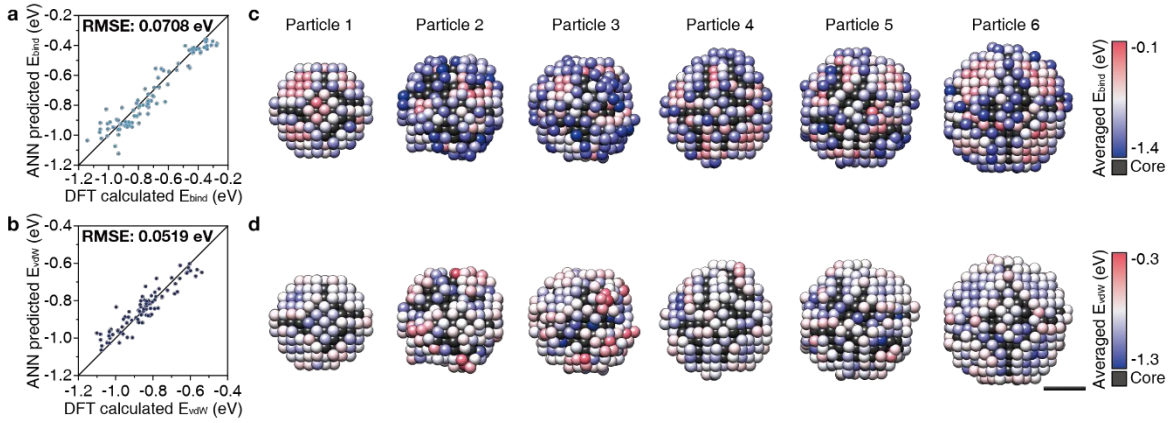

Figure 2. (a, b) Artificial neural network prediction result of the test set for (a) E_{bind} with 0.0708 eV root mean square error and (b) E_{vdW} with 0.0519 eV root mean square error. (c, d) 3D atomic structures of six synthesized Pt nanoparticles colored by (c) θ-averaged E_{bind} and (d) θ-averaged E_{vdW} of PVP ligand. Each Pt nanoparticle has a diameter of 2.25, 2.41, 2.42, 2.52, 2.66, and 2.92 nm, respectively. Scale bar, 1 nm.

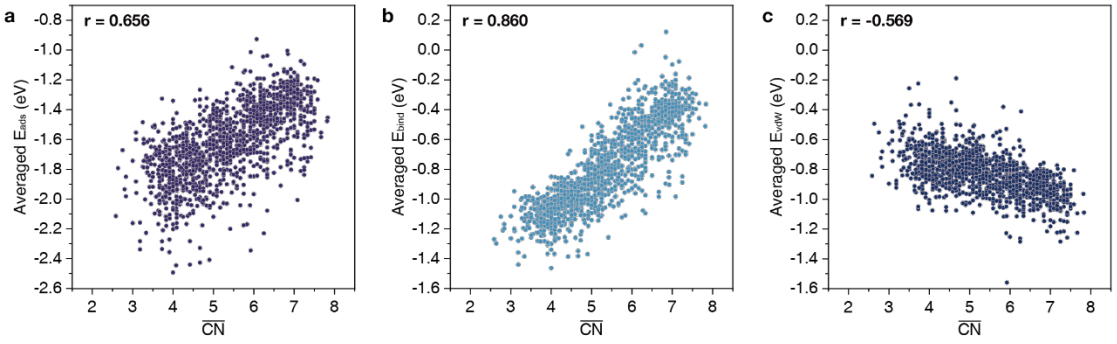

Figure 3. (a) Correlation between $\overline{CN}$ of adsorption centers and θ-averaged adsorption energies predicted by ANN. (b) Correlation between $\overline{CN}$ of adsorption centers and energy contribution of direct bonding. (c) Correlation between $\overline{CN}$ of adsorption centers and energy contribution of van der Waals interaction.

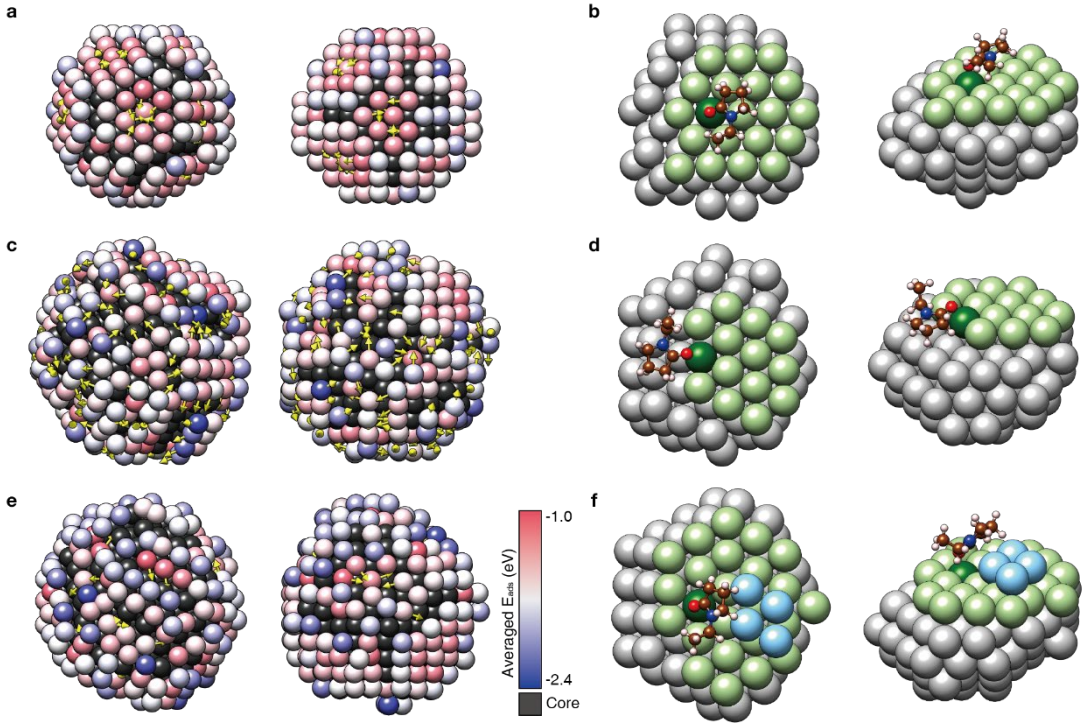

Figure 4. (a, c, e) 3D maps of averaged adsorption energy with yellow arrows indicating characteristic vectors of adsorbed PVP ligands with the lowest E_{vdW}. The PVP ligands are absorbed onto (a) particle 1, (c) particle 5, and (e) particle 4. The arrows come from (a) terraces, (c) edges, corners, and (e) under the islands. (b, d, f) Examples for optimal configurations of PVP ligands absorbed on different surface structures of particle 1, displaying (left) top-view and (right) side-view. The PVP ligands are absorbed on (b) a terrace, (d) an edge, and (f) an under the islands.

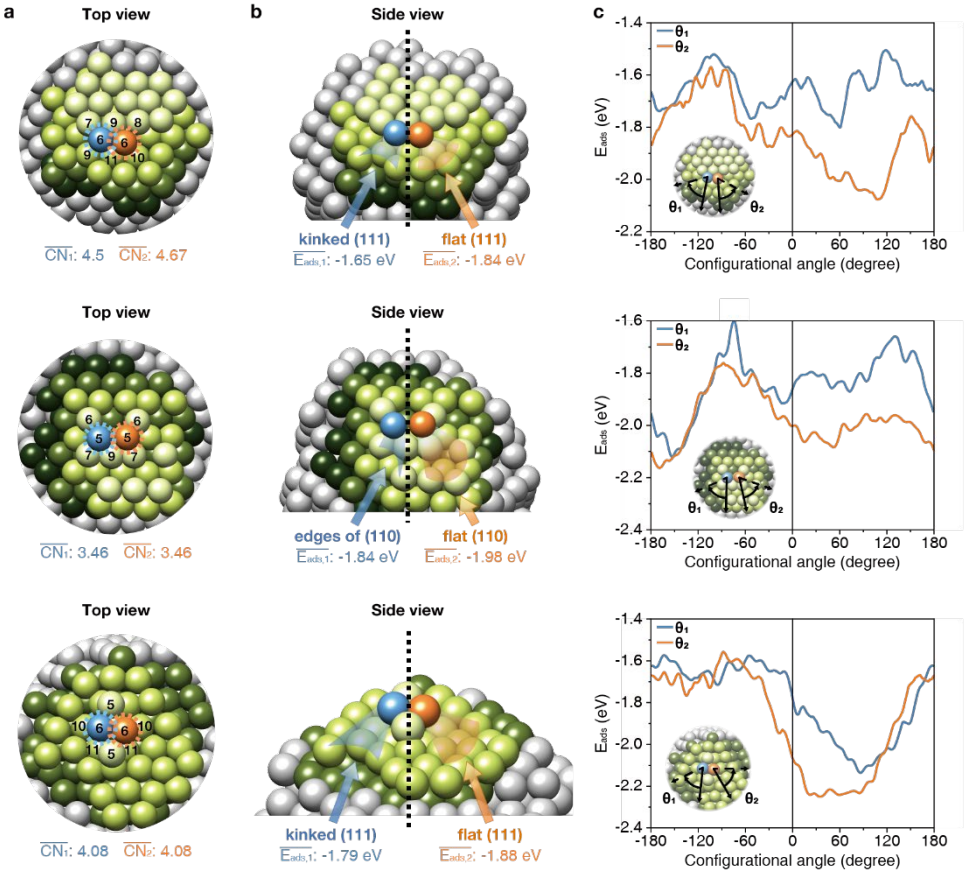

Figure 5. (a) Top view of exemplary adsorption sites with similar $\overline{CN}$ but different adsorption energy. Constituent atoms included in the 10 Å cluster for ANN prediction are colored by depth. The coordination numbers of the adsorption centers and the nearest neighbors of them are indicated. (b) Side view of exemplary adsorption centers. The auxiliary lines are guide for comparing the local geometry of each adsorption site. The θ-averaged adsorption energies of each adsorption center are presented. (c) Angular adsorption energy profiles on each adsorption center.

ASSOCIATED CONTENT

Supporting Information.

The following files are available free of charge.

Methods, supplementary references, and supplementary figures (file type, i.e., PDF)

AUTHOR INFORMATION

Corresponding Authors

Jungwon Park - School of Chemical and Biological Engineering, and Institute of Chemical Processes, Seoul National University, Seoul 08826, Republic of Korea; Center for Nanoparticle Research, Institute for Basic Science (IBS), Seoul 08826, Republic of Korea; Institute of Engineering Research, College of Engineering, Seoul National University, 1 Gwanak-ro, Gwanak-gu, Seoul 151-742, Republic of Korea; Advanced Institutes of Convergence Technology, Seoul National University, 145, Gwanggyo-ro, Yeongtong-gu, Suwon-si, Gyeonggi-do, 16229, Republic of Korea; orcid.org/0000-0003-2927-4331; E-mail: jungwonpark@snu.ac.kr

Hoonkyung Lee - Department of Physics, Konkuk University, Seoul 05029, Republic of Korea; orcid.org/0000-0002-6417-1648; E-mail: hkiee3@konkuk.ac.kr

Sangdeok Shim - Department of Chemistry, Sunchon National University, Suncheon 57922, Republic of Korea; orcid.org/0000-0001-5887-565X; E-mail: san90@scnu.ac.kr

Authors

Dohun Kang - School of Chemical and Biological Engineering, and Institute of Chemical Processes, Seoul National University, Seoul 08826, Republic of Korea; Department of

Materials Science and Engineering, Northwestern University, Evanston, Illinois 60208, USA; orcid.org/0000-0001-5965-6432

Sungin Kim - School of Chemical and Biological Engineering, and Institute of Chemical Processes, Seoul National University, Seoul 08826, Republic of Korea; Center for Nanoparticle Research, Institute for Basic Science (IBS), Seoul 08826, Republic of Korea; orcid.org/0000-0001-9107-0781

Junyoung Heo - School of Chemical and Biological Engineering, and Institute of Chemical Processes, Seoul National University, Seoul 08826, Republic of Korea; Center for Nanoparticle Research, Institute for Basic Science (IBS), Seoul 08826, Republic of Korea; orcid.org/0000-0003-4396-5200

Dongjun Kim - School of Chemical and Biological Engineering, and Institute of Chemical Processes, Seoul National University, Seoul 08826, Republic of Korea; orcid.org/0000-0003-1766-7613

Hyeonhu Bae - Department of Physics, Konkuk University, Seoul 05029, Republic of Korea; orcid.org/0000-0001-7276-6636

Sungsu Kang - School of Chemical and Biological Engineering, and Institute of Chemical Processes, Seoul National University, Seoul 08826, Republic of Korea; Center for Nanoparticle Research, Institute for Basic Science (IBS), Seoul 08826, Republic of Korea; orcid.org/0000-0001-8220-0345

Author Contributions

‖D.K. and S.K. contributed equally to this work. D.K., S.K., and J.P. planned the research. D.K., S.K., J.H., and J.P. acquired the 3D atomic structures. D.K., D.K., and H.B. calculated PVP adsorption energy with DFT. D.K. trained ANN to predict PVP adsorption energy. D.K.,

S.K., J.H., S.K., and J.P. analyzed and interpreted the results. D.K., S.K., J.H., D.K., H.B., S.K., S.S., H.L., and J.P. wrote the manuscript. S.S., H.L., and J.P. supervised the research. All authors contributed to the discussion of results.

Notes

The authors declare no competing financial interest.

ACKNOWLEDGMENT

J.P. acknowledges the Institute for Basic Science (IBSR006-D1). D.K., S.K., J.H., S.K., and J.P. acknowledge the National Research Foundation of Korea (NRF) grant funded by the Korea government (MSIT) (NRF-2020R1A2C2101871). D.K., S.K., J.H., D.K., S.K., and J.P. acknowledge the National Research Foundation of Korea (NRF) grant funded by the Korea government (MSIT) (NRF-2019M3E6A1064877). D.K., S.K., D.K., S.K., and J.P. acknowledge support by Samsung Science and Technology Foundation under project no. SSTFBA1802-08 for sample preparation and method development. J.H., and J.P. acknowledge the National Research Foundation of Korea (NRF) grant funded by the Korea government (MSIT) (NRF-2017R1A5A1015365). Theoretical computation was supported by the National Supercomputing Center with supercomputing resources including technical support (KSC-2020-CRE-0310).

REFERENCES

1. Dong, A.; Ye, X.; Chen, J.; Kang, Y.; Gordon, T.; Kikkawa, J. M.; Murray, C. B., A generalized ligand-exchange strategy enabling sequential surface functionalization of colloidal nanocrystals. *J. Am. Chem. Soc.* **2011**, 133 (4), 998-1006.

2. Yun, H. J.; Paik, T.; Edley, M. E.; Baxter, J. B.; Murray, C. B., Enhanced charge transfer kinetics of CdSe quantum dot-sensitized solar cell by inorganic ligand exchange treatments. *ACS Appl. Mater. & Interfaces* **2014**, 6 (5), 3721-3728.

3. Sheikholeslami, S. N.; Alaeian, H.; Koh, A. L.; Dionne, J. A., A metafluid exhibiting strong optical magnetism. *Nano Lett.* **2013**, 13 (9), 4137-4141.

4. Xia, Y.; Xiong, Y.; Lim, B.; Skrabalak, S. E., Shape-controlled synthesis of metal nanocrystals: simple chemistry meets complex physics? *Angew. Chem. Inter. Ed.* **2009**, 48 (1), 60-103.

5. Xia, X.; Zeng, J.; Oetjen, L. K.; Li, Q.; Xia, Y., Quantitative analysis of the role played by poly (vinylpyrrolidone) in seed-mediated growth of Ag nanocrystals. *J. Am. Chem. Soc.* **2012**, 134 (3), 1793-1801.

6. Geva, N.; Shepherd, J. J.; Nienhaus, L.; Bawendi, M. G.; Van Voorhis, T., Morphology of passivating organic ligands around a nanocrystal. *J. Phys. Chem. C* **2018**, 122 (45), 26267-26274.

7. Ansar, S. M.; Haputhanthri, R.; Edmonds, B.; Liu, D.; Yu, L.; Sygula, A.; Zhang, D., Determination of the binding affinity, packing, and conformation of thiolate and thione ligands on gold nanoparticles. *J. Phys. Chem. C* **2011**, 115 (3), 653-660.

8. Hens, Z.; Martins, J. C., A solution NMR toolbox for characterizing the surface chemistry of colloidal nanocrystals. *Chem. Mater.* **2013**, 25 (8), 1211-1221.

9. De Roo, J.; Ibáñez, M.; Geiregat, P.; Nedelcu, G.; Walravens, W.; Maes, J.; Martins, J. C.; Van Driessche, I.; Kovalenko, M. V.; Hens, Z., Highly dynamic ligand binding and light absorption coefficient of cesium lead bromide perovskite nanocrystals. *ACS Nano* **2016**, 10 (2), 2071-2081.

10. Ye, J.-Y.; Attard, G. A.; Brew, A.; Zhou, Z.-Y.; Sun, S.-G.; Morgan, D. J.; Willock, D. J., Explicit detection of the mechanism of platinum nanoparticle shape control by polyvinylpyrrolidone. *J. Phys. Chem. C* **2016**, 120 (14), 7532-7542.

11. Saidi, W. A.; Feng, H.; Fichthorn, K. A., Binding of polyvinylpyrrolidone to Ag surfaces: Insight into a structure-directing agent from dispersion-corrected density functional theory. *J. Phys. Chem. C* **2013**, 117 (2), 1163-1171.

12. Back, S.; Yeom, M. S.; Jung, Y., Active sites of Au and Ag nanoparticle catalysts for CO2 electroreduction to CO. *ACS Catal.* **2015**, 5 (9), 5089-5096.

13. Back, S.; Kim, H.; Jung, Y., Selective heterogeneous CO2 electroreduction to methanol. *ACS Catal.* **2015**, 5 (2), 965-971.

14. Al-Saidi, W.; Feng, H.; Fichthorn, K. A., Adsorption of polyvinylpyrrolidone on Ag surfaces: insight into a structure-directing agent. *Nano Lett.* **2012**, 12 (2), 997-1001.

15. Gasper, R.; Shi, H.; Ramasubramaniam, A., Adsorption of CO on low-energy, low-symmetry Pt nanoparticles: energy decomposition analysis and prediction via machine-learning models. *J. Phys. Chem. C* **2017**, 121 (10), 5612-5619.

16. Chen, Y.; Huang, Y.; Cheng, T.; Goddard III, W. A., Identifying active sites for CO2 reduction on dealloyed gold surfaces by combining machine learning with multiscale simulations. *J. Am. Chem. Soc.* **2019**, 141 (29), 11651-11657.

17. Gu, G. H.; Lim, J.; Wan, C.; Cheng, T.; Pu, H.; Kim, S.; Noh, J.; Choi, C.; Kim, J.; Goddard III, W. A., Autobifunctional mechanism of jagged Pt nanowires for hydrogen evolution kinetics via end-to-end simulation. *J. Am. Chem. Soc.* **2021**, 143 (14), 5355-5363.

18. Kim, B. H.; Heo, J.; Kim, S.; Reboul, C. F.; Chun, H.; Kang, D.; Bae, H.; Hyun, H.; Lim, J.; Lee, H., Critical differences in 3D atomic structure of individual ligand-protected nanocrystals in solution. *Science* **2020**, 368 (6486), 60-67.

19. Kim, S.; Kwag, J.; Machello, C.; Kang, S.; Heo, J.; Reboul, C. F.; Kang, D.; Kang, S.; Shim, S.; Park, S.-J., Correlating 3D Surface Atomic Structure and Catalytic Activities of Pt Nanocrystals. *Nano Lett.* **2021**, 21 (2), 1175-1183.

20. Behler, J.; Parrinello, M., Generalized neural-network representation of high-dimensional potential-energy surfaces. *Phys. Rev. Lett.* **2007**, 98 (14), 146401.

21. Jiang, T.; Mowbray, D.; Dobrin, S.; Falsig, H.; Hvolbæk, B.; Bligaard, T.; Nørskov, J. K., Trends in CO oxidation rates for metal nanoparticles and close-packed, stepped, and kinked surfaces. *J. Phys. Chem. C* **2009**, 113 (24), 10548-10553.

22. Calle-Vallejo, F.; Tymoczko, J.; Colic, V.; Vu, Q. H.; Pohl, M. D.; Morgenstern, K.; Loffreda, D.; Sautet, P.; Schuhmann, W.; Bandarenka, A. S., Finding optimal surface sites on heterogeneous catalysts by counting nearest neighbors. *Science* **2015**, 350 (6257), 185-189.

23. Calle-Vallejo, F.; Pohl, M. D.; Bandarenka, A. S., Quantitative coordination–activity relations for the design of enhanced Pt catalysts for CO electro-oxidation. *ACS Catal.* **2017**, 7 (7), 4355-4359.

24. Han, B.; Miranda, C.; Ceder, G., Effect of particle size and surface structure on adsorption of O and OH on platinum nanoparticles: A first-principles study. *Phys. Rev. B* **2008**, 77 (7), 075410.

25. Calle-Vallejo, F.; Loffreda, D.; Koper, M.; Sautet, P., Introducing structural sensitivity into adsorption–energy scaling relations by means of coordination numbers. *Nat. Chem.* **2015**, 7 (5), 403-410.

26. Qiu, L.; Liu, F.; Zhao, L.; Yang, W.; Yao, J., Evidence of a unique electron donor− acceptor property for platinum nanoparticles as studied by XPS. *Langmuir* **2006**, 22 (10), 4480-4482.